

# A New Set of Classical-Like Mass Assignment Schemes for Power Spectrum Estimation

O. N. Gomez-Giraldo 1 and J. C. Muñoz-Cuartas ©1

<sup>1</sup>Grupo de Física y Astrofísica Computacional (FACom), Instituto de Física, Facultad de Ciencias Exactas y Naturales, Universidad de Antioquia, Calle 70 No. 52-21, Medellín, Colombia.

Keywords: cosmology: large-scale, cosmology: miscellaneous, methods: numerical, structure of Universe

## **Abstract**

In this study, we present the impact of the mass-assignment scheme (MAS) on the estimation of the power spectrum and bispectrum in simulations of structure formation. We used numerical simulations to study the aliasing effect for both power spectrum and bispectrum estimation using the classical MAS, such as Nearest Grid Point, Cloud In Cell, and Triangular Shaped Cloud, to estimate, which suffers from a smaller aliasing effect for both small and large scales. We propose a new set of MAS, the NJ1, NJ2, and NJ3 functions, and study its aliasing effect, obtaining an improvement with respect to the classical schemes without the need for additional computational resources. We show that with the newly proposed MAS, we achieve comparable or even better performance in the aliasing of the power spectrum and bispectrum at the expense of a lower computational cost compared to high-order interpolation schemes such as PCS, resulting in an effective improvement in the estimation of the power spectrum and bispectrum.

#### Resumen

En este trabajo se estudia el impacto del esquema de asignación de masa (MAS) en la estimación del espectro de potencias y el biespectro en simulaciones de formación de estructuras. Se usan simulaciones numéricas para estudiar el aliasing effect para el espectro de potencias y el biespectro usando esquemas clásicos de asignación de masa como Nearest Grid Point, Cloud In Cell y Triangular Shaped Cloud con el ánimo de determinar cuál sufre del menor aliasing effect en grandes y pequeñas escalas. Proponemos un nuevo conjunto de MAS, las funciones NJ1, NJ2 y NJ3 y estudiamos su aliasing effect, obteniendo una mejoría en relación con los esquemas clásicos a expensas de un menor costo computacional. Mostramos que con estos nuevos MAS, se alcanzan resultados comparables, o mejores, en la estimación del espectro de potencia y biespectro a un costo computacional reducido, cuando se le compara con funciones de interpolación de orden superior como PCS, resultando en una mejora efectiva en la estimación del espectro de potencia y biespectro.

# 1. Introduction

Large-scale structure (LSS) is believed to form from primordial fluctuations caused by gravitational instabilities in the early Universe (Scoccimarro, 1997). In order to characterize quantitatively the clustering of these structures, different statistical methods are used to infer properties that can give constraints to cosmological models as well to cosmological parameters (e.g. Gil-Marín et al., 2015). Because the statistical independence of the Fourier modes of a homogeneous random field, these statistics are expressed in Fourier space, making the study of these fields easier (e.g. Peebles, 1980; Martínez & Saar, 2002).

The matter power spectrum is one of the most common statistical measures of gravitational clustering. Its importance lies in the fact that for a Gaussian random field, the power spectrum describes completely its statistical properties (Bernardeau et al., 2002). Nonetheless, a complete description for a non-Gaussian distribution, which can be primordial or can emerge from non-

linear processes, requires the use of higher-order correlation functions (Peebles, 1980). The bispectrum is a standard probe for studying non-Gaussianities in the LSS. It is the lowest-order indicator of this kind of these features in the primordial density field, providing constraints on inflationary models and insights into non-linear phenomena such as structure formation and galaxy bias (e.g. Scoccimarro, 2000; Gil-Marín et al., 2015).

The problem of measuring Fourier mode statistics from a distribution of points – as the case of N-body simulations or galaxy surveys – is taking great importance, particularly, in the context of the one-percent accuracy era. Fourier mode statistics involves the use of a mass assignment scheme, which interpolates the point mass distribution onto a regular grid, to then compute a fast Fourier transform. Nevertheless, this sampling to a regular grid results in a convolution with a window function and a product with a sampling function (Jing, 2005; Sefusatti et al., 2016). Therefore, two effects are introduced; a decreasing of the modes at small scales and aliasing due to the finite resolution of the grid (Hockney & Eastwood, 1981; Colombi et al., 2009).

Besides, there is an additional term induced because of the discreteness of the distribution. The shot-noise term can be easily corrected but the aliasing effect is not straightforward to deal with. Jing (2005) derived an expression for the aliasing in the power spectrum independent of the window function. This iterative method corrects the aliasing effect but cannot be applied to the bispectrum. Colombi et al. (2009) proposed a method to estimate the Fourier coefficients based on the Taylor expansion of the trigonometric functions and developed a public tool, POWMES. Sefusatti et al. (2016) employed a procedure that interlaces two density grids to remove alias contribution, which led to errors for the Cloud-In-Cell method nearly below 0.1 percent for the power spectrum up to the Nyquist wavenumber and below 0.1 percent for  $k \le (2/3) k_N$ , but at the cost of doubling the number of operations and the amount of memory required. Cui et al. (2008) proposed instead a desirable window function in which the effect of aliasing is reduced, particularly, they used the scaling functions of the Daubechies wavelet transform, getting an error in the power spectrum estimation with respect to theoretical predictions below 2 percent for  $k \le 0.7 k_{\rm N}$ , but they did not do an analysis with respect to an alias-free estimation neither they try to use this kind of mass assignment scheme for bispectrum estimation, even so, they claimed it as a good mass-assignment scheme for Fourier statistics.

In this work, we study systemically the effect of aliasing effect in the power spectrum and bispectrum for the traditional mass assignment schemes (MAS), Nearest Grid Point (NGP), Cloud In Cell (CIC) and Triangular Shaped Cloud (TSC). Then, we propose a set of new mass assignment schemes: the NJ1, NJ2, and NJ3 functions, aiming to improve with respect the classical mass assignment schemes without the need of more computational resources. The structure of the paper is as follows: First, an introduction to the problem is presented. Next, in § 2 and 3 we present definitions and the formalism associated with the estimation of Fourier statistics of the density field. Then in § 4 we present our proposal for a new set of MAS, the NJ functions, namely, NJ1, NJ2, and NJ3. In § 5 and 6 we describe our numerical experiments an results on the estimation of the power spectrum and bispectrum for the new MAS functions, NJ1, NJ2, and NJ3. Finally, § 7 presents the results and conclusions of this study.

### 2. Fourier statistics

At large-scales, LSS dynamics is governed by its density contrast  $\delta(\mathbf{x})$ , with the matter distribution given by  $\rho(\mathbf{x}) = \overline{\rho} \left[ 1 + \delta(\mathbf{x}) \right]$  (Bernardeau et al., 2002). Statistical tools are used to study the properties of fields with cosmological fluctuations owing to the lack of direct observational access. The large time scales involved make it impossible to track the temporal evolution of individual systems (Bernardeau et al., 2002; Martínez & Saar, 2002). The initial density fluctuation is modeled as a realization of an ensemble (Fry, 1984). Additionally, as a consequence of the cosmological principle, the matter density field has the property of being statistically homogeneous and isotropic (Mo, van den Bosch, & White, 2010).

Knowledge of distinct large-scale statistical properties can provide information about the nature of primordial overdensities, different possible inflationary scenarios, as well as give constraints on cosmological parameters and information about different nonlinear phenomena such as gravity. The probability distribution function is completely described by its moments, which are

defined as the expected values of the product of the fields at different points of space (Mo et al., 2010; Gil-Marín et al., 2014).

## 2.1. Fourier representation

Density fluctuations are usually described in terms of its Fourier components,

$$\delta(\mathbf{k}) = \int d^3 \mathbf{x} \, \delta(\mathbf{x}) \, e^{-i\mathbf{k} \cdot \mathbf{x}},\tag{1}$$

where the integral is taken over the volume  $V=L^3$ . Under these conditions, the perturbation field can be assumed as periodic and with  $\mathbf{k}=k_{\rm f}\mathbf{n}=k_{\rm f}(i_x,i_y,i_z)$ , with  $k_{\rm f}=2\pi/L$  the fundamental frequency and  $i_x,i_y,i_z$  integer numbers.

Additionally, we can define the Dirac delta function as

$$\delta^{D}(\mathbf{k}) = \int \frac{\mathrm{d}^{3}\mathbf{x}}{(2\pi)^{3}} \,\mathrm{e}^{\pm\mathrm{i}\mathbf{k}\cdot\mathbf{x}} \tag{2}$$

and its discrete version, the Kronecker delta,

$$\delta_{\mathbf{k}}^{K} = \begin{cases} 1 & \text{if } \mathbf{k} = \mathbf{0} \\ 0 & \text{otherwise,} \end{cases}$$
 (3)

such that the continuous limit is recovered for  $V \to \infty$  (or  $k_{\rm f} \to 0$ ) with (Sefusatti et al., 2016)

$$\lim_{k_{\rm f}\to 0} \frac{\delta_{\mathbf{k}}^K}{k_{\rm f}^3} = \delta^D(\mathbf{k}). \tag{4}$$

The reason to work in Fourier space is because it allows to separate  $\delta$  according to the scale, preserving its statistical properties. As  $\delta(\mathbf{x})$  is a real quantity, we have that  $\delta(\mathbf{k})$  is hermitian, i.e.,  $\delta(\mathbf{k}) = \delta^*(-\mathbf{k})$ , consequently, we only need the upper (or lower) half space to completely specify  $\delta(\mathbf{x})$  (Mo et al., 2010).

# 2.2. Power spectrum

The power spectrum P(k) is the simplest Fourier statistic that allows to characterize the clustering pattern of the matter density field. It is the Fourier transform of the two point correlation function and is defined as

$$\langle \delta(\mathbf{k}_1)\delta(\mathbf{k}_2)\rangle = (2\pi)^3 \,\delta^D \left(\mathbf{k}_1 + \mathbf{k}_2\right) P(k_1),\tag{5}$$

where the Dirac delta function indicates the connected part between wavevectors  $\mathbf{k}_1$  and  $\mathbf{k}_2$ . The symbol  $\langle \cdots \rangle$  denotes the ensemble average over independent realizations of the Universe, under the ergodicity hypothesis the average over different directions of  $\mathbf{k}$  will give the same resulting in an ensemble average (Gil-Marín et al., 2012).

The power spectrum is the Fourier transform of the two point correlation function, which is related to the second moment of the random field  $\delta$ . Because of this, it is common to use power spectra as a tool to characterize the clustering pattern, in particular, in the large scales, where different modes can be treated independently. For a Gaussian random field the power spectrum describes the statistical features of the data. The galaxy power spectrum has been extensively used in the literature to constraint structure formation, cosmological parameters as well as galaxy bias models, giving valuable information that helped to establish the  $\Lambda$ CDM as the standard cosmological model (see Gil-Marín et al., 2012; Martínez & Saar, 2002; Bernardeau et al., 2002, and references therein).

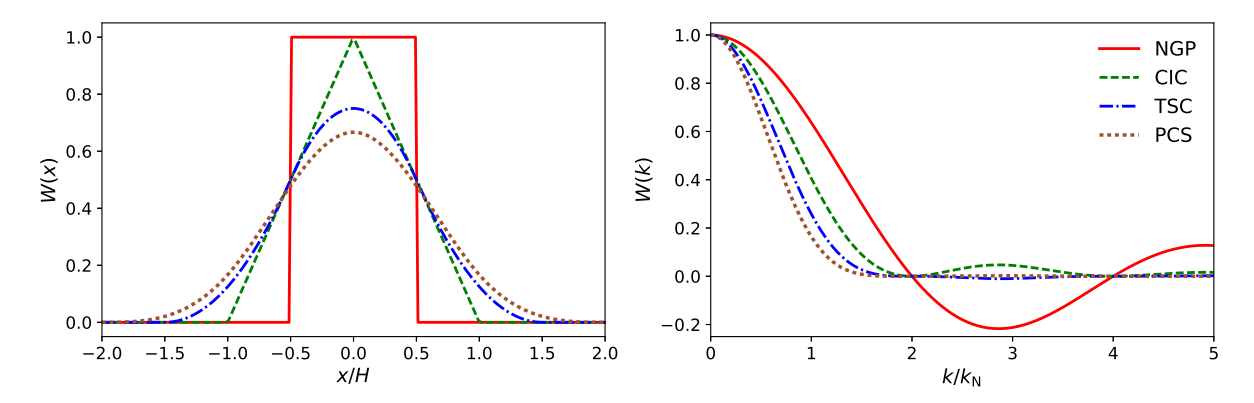


**Figure 1.** Left panel: One-dimensional window function in real space W(x) of the classical mass assignment schemes NGP, CIC, TSC, and PCS. Right panel: the same window functions in Fourier space W(k).

## 2.3. Bispectrum

When a random field is not-Gaussian, it is necessary to use higher-order correlation functions to characterize their statistical properties. The next statistic of interest is the bispectrum or the three-point correlation function in Fourier space, defined as

$$\langle \delta(\mathbf{k}_1)\delta(\mathbf{k}_2)\delta(\mathbf{k}_3)\rangle = (2\pi)^3 \,\delta^D(\mathbf{k}_1 + \mathbf{k}_2 + \mathbf{k}_3) B(k_1, k_2, k_3). \quad (6)$$

For this case, the Dirac delta demands that the bispectrum has to be non-zero only for wavevector configurations that make closed triangles, i.e.,  $\mathbf{k}_1 + \mathbf{k}_2 + \mathbf{k}_3 = 0$ . Note that the product  $\delta(\mathbf{k}_1)\delta(\mathbf{k}_2)\delta(\mathbf{k}_3)$  is in general a complex number but, because the hermiticity of  $\delta(\mathbf{k})$ , once the mean is taken the imaginary part goes to zero (Gil-Marín et al., 2012).

It is usual to define the reduced bispectrum Q as

$$Q(k_1, k_2, k_3) = \frac{B(k_1, k_2, k_3)}{P(k_1)P(k_2) + P(k_2)P(k_3) + P(k_3)P(k_1)}.$$
 (7)

Although this quantity does not give any additional information to the power spectrum and bispectrum, it has been historically used in cosmology because is the associated hierarchical amplitude for the bispectrum and its weakly dependence on cosmology and scale.

For a Gaussian random field the bispectrum is null, therefore, it could help to study primordial non-Gaussianity which opens the possibility to distinguish between different inflationary models (Schmittfull, Regan, & Shellard, 2013). In addition, whether or not the random field is initially Gaussian or not, when nonlinear processes – such as gravitational collapse – are present, they introduce non-Gaussianities, allowing bispectrum to be used to extract information on non-linearities in galaxy clustering. Besides, galaxy biasing also introduce non-linear effects in the density field, letting us to use bispectrum as an important tool to study galaxy bias at large scales (Matarrese et al., 1997; Gil-Marín et al., 2015).

# 3. Mass assignment schemes and aliasing

#### 3.1. Classical mass assignment schemes

In order to use Fast Fourier transform algorithms, it is necessary to sample mass density into a regular grid. This is done by spreading out the particle distribution to the desired grid points with the help of mass assignment scheme (MAS).

For a distribution of points with  $N_p$  particles, the grid mass at  $\mathbf{x}_g$  is given by

$$\widetilde{m}(\mathbf{x}_{g}) = \sum_{i=1}^{N_{p}} m_{i} W(\mathbf{x}_{g} - \mathbf{x}_{i}), \qquad (8)$$

with  $m_i$  and  $\mathbf{x}_i$  the mass and position of the i-th particle. The mass assignment to a grid-point  $\mathbf{x}_{\mathrm{g}}$  is formulated as a convolution of the mass density with a window function W (Jeong, 2010). The window function quantifies how mass is distributed to a grid point separated by a distance  $|\mathbf{x}_{\mathrm{g}} - \mathbf{x}'|$ . The sampling of the convolved density contrast to a regular grid of size  $N^3$  is simply

$$\widetilde{\delta}(\mathbf{x}_{\mathrm{g}}) = \frac{\widetilde{\rho}(\mathbf{x}_{\mathrm{g}})}{\overline{\rho}} - 1. \tag{9}$$

Because of the convolution theorem, the resulting Fourier transform of the density contrast is

$$\widetilde{\delta}(\mathbf{k}) = \delta(\mathbf{k}) W(\mathbf{k}). \tag{10}$$

The window function can be represented in an unique way given a mass assignment scheme by means of the integral of the cell volume centered at  $\mathbf{x}_g$  of the so-called shape function  $S(\mathbf{x})$  (Hockney & Eastwood, 1981; Jeong, 2010). For the one-dimensional case we have

$$W(x) = \frac{1}{H} \int_{x_0 - H/2}^{x_g + H/2} dx' S(x' - x), \tag{11}$$

where H = L/N is the grid size. With the definition of the top-hat function  $\Pi(x)$ ,

$$\Pi(x) = \begin{cases} 1 & \text{if } |x| < 1/2\\ 1/2 & \text{if } |x| = 1/2\\ 0 & \text{otherwise} \end{cases}$$
 (12)

Gomez-Giraldo et al

and constraining S to even functions, we can write (11) as

$$W(x) = \frac{1}{H} \int dx' \,\Pi\left(\frac{x'}{H}\right) S(x - x') = \frac{1}{H} \Pi\left(\frac{x}{H}\right) * S(x). \quad (13)$$

Therefore, the window function corresponds to the convolution of the shape function using a top-hat function. The most common classical mass assignment schemes are the Nearest Grid Point (NGP), Cloud In Cell (CIC), Triangular Shaped Cloud (TSC) and Piece-wise Spline (PCS), where

• NGP  $W_{\text{NGP}}(x) = \begin{cases} 1 & \text{if } |x| < H/2 \\ 1/2 & \text{if } |x| = H/2 \\ 0 & \text{otherwise.} \end{cases}$  (14)

• CIC 
$$W_{\text{CIC}}(x) = \begin{cases} 1 - |x|/H & \text{if } |x| < H \\ 0 & \text{otherwise.} \end{cases}$$
 (15)

TSC

$$W_{\text{TSC}}(x) = \begin{cases} \frac{3}{4} - \left(\frac{x}{H}\right)^2 & \text{if } |x| \le \frac{H}{2} \\ \frac{1}{2} \left(\frac{3}{2} - \frac{|x|}{H}\right) & \text{if } \frac{H}{2} \le |x| \le \frac{3H}{2} \\ 0 & \text{otherwise.} \end{cases}$$
(16)

PCS

$$W_{PCS}(x) = \begin{cases} \frac{2}{3} - \left(\frac{x}{H}\right)^2 + \frac{1}{2} \left(\frac{|x|}{H}\right)^3 & \text{if } |x| < H\\ \frac{1}{6} \left(2 - \frac{|x|}{H}\right)^3 & \text{if } H \le |x| < 2H\\ 0 & \text{otherwise.} \end{cases}$$
(17)

The three-dimensional form of the window function in real space is given as  $W(\mathbf{x}) = W(x)W(y)W(z)$ . Given a wavevector  $\mathbf{k}$ , the Fourier transform of the window functions for the classical mass assignment schemes is

$$W(\mathbf{k}) = \left[ \frac{\sin(\pi k_x / 2k_N) \sin(\pi k_y / 2k_N) \sin(\pi k_z / 2k_N)}{(\pi k_x / 2k_N) (\pi k_y / 2k_N) (\pi k_z / 2k_N)} \right]^p, \quad (18)$$

with p either 1, 2, 3 or 4 for NGP, CIC, TSC, and PCS, respectively and  $k_{\rm N}=\pi/H$  is the Nyquist wavenumber.

In the left panel of Figure 1 we show the one-dimensional form of these window functions in real space while in the right panel we show the corresponding window functions in Fourier space.

# 3.2. Aliasing

The fast Fourier transformed density contrast must be previously sampled from a homogeneous grid. This sampling can be mathematically expressed in real space by means of the so-called sampling function (Jeong, 2010; Sefusatti et al., 2016; Hockney & Eastwood, 1981), defined as

$$III(\mathbf{x}) = \sum_{\mathbf{n}} \delta^{D}(\mathbf{x} - \mathbf{n}), \tag{19}$$

with n being an integer vector. Thus, we can express the sampled field compactly as

$$\widetilde{\delta}^{G}(\mathbf{x}) = \operatorname{III}\left(\frac{\mathbf{x}}{H}\right) \left[\delta(\mathbf{x}) * W(\mathbf{x})\right].$$
 (20)

By means of the convolution theorem we have

$$\widetilde{\delta}^{G}(\mathbf{k}) = k_{f}^{3} \sum_{\mathbf{k}'} III(\mathbf{k}') \, \widetilde{\delta}(\mathbf{k} - \mathbf{k}'), \tag{21}$$

with  $\widetilde{\delta}(\mathbf{k})$  the Fourier transform of the convolved density field, the superscript G means that the density contrast was sampled on a regular grid. The Fourier transform of a sampling function is also a sampling function (with the appropriate periodic conditions in the Fourier representation). Because of the  $2k_{\rm N}$  periodicity we have then

$$III(\mathbf{k}) = \frac{1}{k_f^3} \sum_{\mathbf{n}} \delta_{\mathbf{k}+2k_N \mathbf{n}}^K.$$
 (22)

As a consequence, we have (see Sefusatti et al., 2016)

$$\widetilde{\delta}^{G}(\mathbf{k}) = \sum_{\mathbf{n}} \widetilde{\delta}(\mathbf{k} + 2k_{N}\mathbf{n}) = \sum_{\mathbf{n}} W(\mathbf{k} + 2k_{N}\mathbf{n})\delta(\mathbf{k} + 2k_{N}\mathbf{n}).$$
(23)

Therefore, the finite sampling of the convolved density field becomes a sum of aliasing contributions, which is more significant near to the Nyquist wavenumber and has to be corrected for a precise estimation. The "corrected" grid-sampled density contrast is obtained by dividing with the window function in Fourier space,

$$\delta^{G}(\mathbf{k}) = \frac{\widetilde{\delta}^{G}(\mathbf{k})}{W(\mathbf{k})} = \delta(\mathbf{k}) + \sum_{\mathbf{n} \neq 0} w_{\mathbf{n}}(\mathbf{k}) \, \delta(\mathbf{k} + 2k_{N}\mathbf{n}), \tag{24}$$

with  $w_{\mathbf{n}}(\mathbf{k}) = W(\mathbf{k} + 2k_{\mathrm{N}}\mathbf{n})/W(\mathbf{k})$ . The term  $\mathbf{n} = \mathbf{0}$  provides the desired density contrast  $\delta(\mathbf{k})$ , while other terms mean that values outside of the The Nyquist wavenumber was incorrectly moved within this range. These unwanted contributions to the density contrast due to the alias sum are related with both the small-scale features and with the value of the  $w_{\mathbf{n}}(\mathbf{k})$  ratio.

Aliasing also affects the estimated power spectrum such that the "deconvolved" estimation is given by (Jing, 2005)

$$P^{G}(k) = P^{d}(k) + \sum_{\mathbf{n} \neq \mathbf{0}} \left| w_{\mathbf{n}}(\mathbf{k}) \right|^{2} P^{d} \left( \left| \mathbf{k} + 2k_{N} \mathbf{n} \right| \right), \tag{25}$$

with

$$P^{d}(k) = P(k) + P_{SN},$$
 (26)

being  $P_{\rm SN}=1/\overline{n}$  the discreteness or shot-noise term. For bispectrum, the aliasing effect, with  $B_{123}^{\rm G}=B^{\rm G}({\bf k}_1,{\bf k}_2,{\bf k}_3)$ , is given by

$$B_{123}^{G} = \sum_{\mathbf{n}_{1}, \mathbf{n}_{2}, \mathbf{n}_{3}} w_{\mathbf{n}_{1}}(\mathbf{k}) w_{\mathbf{n}_{2}}(\mathbf{k}) w_{\mathbf{n}_{3}}(\mathbf{k}) B^{d}(\mathbf{k}'_{1}, \mathbf{k}'_{2}, \mathbf{k}'_{3}),$$
(27)

with  $\mathbf{k}_i' = \mathbf{k}_i + 2k_N \mathbf{n}_i$  and

$$B^{d}(\mathbf{k}_{1}, \mathbf{k}_{2}, \mathbf{k}_{3}) = B(\mathbf{k}_{1}, \mathbf{k}_{2}, \mathbf{k}_{3}) + B_{SN}(\mathbf{k}_{1}, \mathbf{k}_{2}, \mathbf{k}_{3}), \tag{28}$$

where  $B_{SN}(\mathbf{k}_1, \mathbf{k}_2, \mathbf{k}_3) = [P(k_1) + P(k_2) + P(k_3)]/\overline{n} + 1/\overline{n}^2$  is bispectrum-associated shot noise term. For both power spectrum and bispectrum, we have to deconvolve the window function. This is because of the imprint of the mass assignment scheme in these quantities. Consequently, when using a MAS, the measured power spectrum and bispectrum are biased estimations of the real functions. The measured quantity is a statistic of the density contrast convolved with the window function and the so-called sampling function. Therefore, the estimated power spectrum and bispectrum will show an artificial suppression mainly noted at

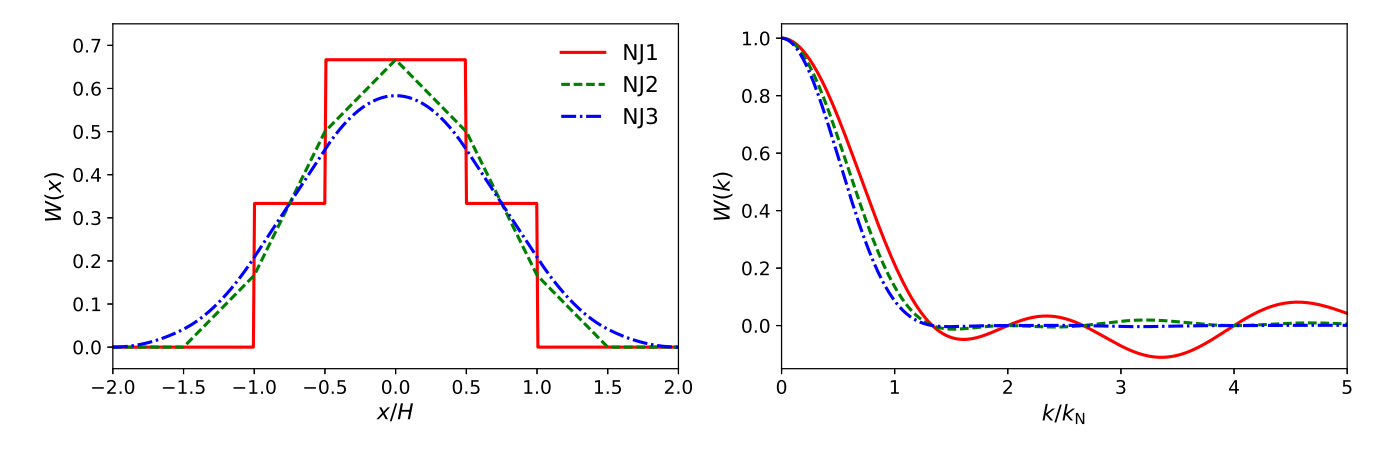


**Figure 2.** Left panel: one-dimensional plot of the modified version of classical mass-assignment schemes in real space. Right panel: associated window functions in Fourier space.

 $k \gtrsim 0.7 k_{\rm N}$  (Jeong, 2010; Sefusatti et al., 2016; Hockney & Eastwood, 1981).

# 4. Derived classical-like mass assignment schemes

The definition of the new mass assignment schemes proposed for this work lies on classical ones such as NGP, CIC, and TSC. We define them as

$$W(x) = \frac{1}{3} \left[ W^{\text{cl}}\left(x - \frac{1}{2}\right) + W^{\text{cl}}\left(x\right) + W^{\text{cl}}\left(x + \frac{1}{2}\right) \right], \quad (29)$$

where  $W^{cl}(x)$  refers to the window function of a given classical mass assignment scheme. According to the mass assignment scheme used, the derived schemes are called NJ1 for NGP, while NJ2 and NJ3 for CIC and TSC schemes. With this, the precise definition of the The newly derived mass assignment schemes are presented in Eqs. 30, 31 and 32, respectively.

$$W_{\text{NJI}}(x) = \frac{1}{3} \left[ W_{\text{NGP}}(x - 1/2) + W_{\text{NGP}}(x) + W_{\text{NGP}}(x + 1/2) \right]$$

$$= \frac{1}{3} \begin{cases} 2 & \text{if } |x| < \frac{1}{2} \\ \frac{3}{2} & \text{if } |x| = \frac{1}{2} \\ 1 & \text{if } \frac{1}{2} < |x| < 1 \\ \frac{1}{2} & \text{if } |x| = 1 \\ 0 & \text{otherwise,} \end{cases}$$
(30)

$$W_{\text{NJ2}}(x) = \frac{1}{3} \left[ W_{\text{CIC}}(x - 1/2) + W_{\text{CIC}}(x) + W_{\text{CIC}}(x + 1/2) \right]$$

$$= \frac{1}{3} \begin{cases} 2 - |x| & \text{if } |x| < \frac{1}{2} \\ \frac{5}{2} - 2|x| & \text{if } \frac{1}{2} \le |x| < 1 \\ \frac{3}{2} - |x| & \text{if } 1 \le |x| < \frac{3}{2} \\ 0 & \text{otherwise,} \end{cases}$$
(31)

$$W_{\text{NJ3}}(x) = \frac{1}{3} \left[ W_{\text{TSC}}(x - 1/2) + W_{\text{TSC}}(x) + W_{\text{TSC}}(x + 1/2) \right]$$

$$= \frac{1}{3} \begin{cases} \frac{7}{4} - \frac{3}{2}x^2 & \text{if } |x| \le \frac{1}{2} \\ \frac{17}{8} - \frac{3}{2}|x| & \text{if } \frac{1}{2} < |x| \le 1 \\ x^2 - \frac{7}{2}|x| + \frac{25}{8} & \text{if } 1 < |x| \le \frac{3}{2} \\ \frac{x^2}{2} - 2|x| + 2 & \text{if } \frac{3}{2} < |x| \le 2 \\ 0 & \text{otherwise.} \end{cases}$$
(32)

The left panel of Fig. 2 shows a one-dimensional plot of these new window functions. By comparing with Figure 1, we can observe that these newly derived mass assignment schemes spread as the next-order interpolator of the progenitor mass assignment scheme. For instance, the NJ2 function spreads like that of TSC. However, these new mass assignment schemes run faster than the next-order classical interpolator because our new mass assignment schemes inherit the operation order of the progenitor mass assignment schemes, making them run even until 60% of the next-order progenitor interpolator time.

By making use of the modulation theorem, the Fourier transform of these modified window functions are given by

$$W(k) = \frac{1}{3} \left[ \frac{\sin\left(\frac{\pi k}{2k_N}\right)}{\left(\frac{\pi k}{2k_N}\right)} \right]^p \left\{ 2\cos\left(\frac{\pi k}{2k_N}\right) + 1 \right\},\tag{33}$$

with p=1, 2, 3 for the NJ1, NJ2 and NJ3 window functions respectively, in the left panel of Figure 2 we show the plot of the one-dimensional Fourier transform for each derived window function, again by comparing with the right panel of Figure 1 we can see how there is a suppression of wings associated with aliasing owing to the modulation of window function.

Again, the advantage of these modified classical-like mass assignment schemes is that there is a reduction in the aliasing contribution owing to the modulation given by the cosine factor in (33). In Figure 3 we show the alias contributions of the classical MAS and our derived versions. For this, we use an estimator given by the residual terms due to the alias contribution defined as  $\sum_{n\neq 0} |W(k+2k_n n)/W(k)|^2 \text{ (Sefusatti et al., 2016); if the residual contribution is higher, then the alias contribution increases. For each of the derived schemes we got for the residuals at <math>k \sim 0.7k_N$  an improvement even close to two orders of magnitude with

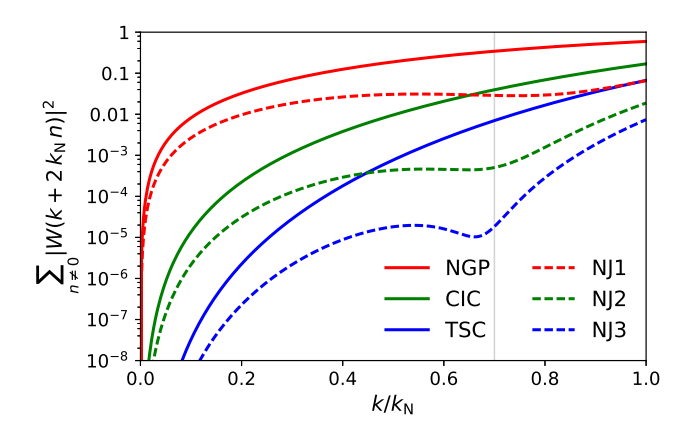


**Figure 3.** Plot of the one-dimensional residual induced by the alias sum of the classical MAS and the derived MAS studied in this work.

Table 1. Cosmological Parameters

$\Omega_{\Lambda}$	0.742
$\Omega_{ m m}$	0.258
$\Omega_{ m b}$	0.0438
h	0.72
$n_{\rm s}$	0.96
$\sigma_8(z=0)$	0.796
$m_{ m p}$	$3.4145 \times 10^{10} \; \mathrm{M}_{\odot}$
	<u> </u>

respect to their corresponding progenitor MAS, providing an initial perspective on the use of these derived functions.

# 5. N-body simulations

The simulation used for this work consisted of a cosmological box of size  $L = 400 \,\mathrm{Mpc} \,\mathrm{h}^{-1}$ , with a particle number of  $N_{\mathrm{p}} = 512^3$  which was performed using the code GADGET2 (Springel, 2005), with the cosmological parameters summarized in Table 1.

Due to the computation time, from the cosmological box we estimated the Fourier transform by direct method as

$$\delta(\mathbf{k}) = \frac{1}{\bar{n}} \sum_{i=1}^{N_{p}} e^{-i\mathbf{k} \cdot \mathbf{x_{i}}} - V \delta_{\mathbf{k}}^{K}, \tag{34}$$

where we used the Kronecker delta  $\delta_{\mathbf{k}}^{K}$ , defined to be one for k=0 and zero otherwise, and  $\bar{n}=N_{\mathrm{p}}/V$ .

For our estimates we used a mesh with a number of grids of  $N_{\rm g}^3=64^3$ . Therefore, the results associated with FFT using different MAS will also have the same number of grids. For this box the associated fundamental wavenumber is given by  $k_f=(2\pi)/L\approx 0.0157\,{\rm h\,Mpc^{-1}}$  and, with the given number of grids, the associated Nyquist wavenumber is  $k_{\rm N}=(\pi\,N_{\rm g})/L\approx 0.5027\,{\rm h\,Mpc^{-1}}$ .

# 6. Results

## 6.1. Aliasing contribution on power spectrum

In this part we are going to test the effect of the aliasing on the estimation of the power spectrum for these new derived window functions

In Figure 4 we show the absolute deviation of different mass assignment schemes studied in this work against the result of the

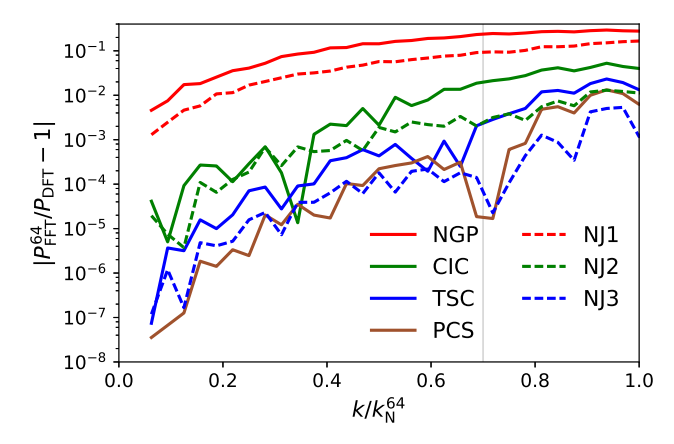


**Figure 4.** Aliasing contribution on power spectrum. We show the power spectrum obtained by taking FFT with different MAS against the estimation with FT by direct summation. Filled lines represent traditional mass assignment schemes, NGP (red), CIC (green) and TSC (blu), while the plot we show the absolute value deviation for different mass assignment schemes with respect to the alias-free Fourier transform. All estimations were performed with N-body simulation with parameters described in Table 1.

Fourier transform using a direct sum. For a better comparison, we also include the deviation for the next order interpolator of the TSC function, the Piecewise Cubic Spline (PCS; Sefusatti et al., 2016). We found for the power spectrum a systematic improvement for our modified versions with results of the same order to the next order mass assignment scheme of the progenitor window function, reaching absolute deviations at  $k=0.7k_N$  of 20%, 2%, 0.2%, 0.01% for the NGP, CIC, TSC and PCS window function respectively while for our modified versions we got a deviation of 9%, 0.3% and 0.008% for NJ1, NJ2 and NJ3 respectively. Therefore, with the NJ functions we are obtaining comparable contributions for the aliasing than the next order function for the progenitor MAS which means we are reaching a more accurate value for the power spectrum at the expenses of a lower computational cost.

# 6.2. Aliasing contribution on bispectrum

In Figure 5 we show how aliasing works on the bispectrum for our modified mass assignment schemes, NJ1, NJ2, NJ3, compared with those of NGP, CIC, TSC, and PCS. Following (Sefusatti et al., 2016), for the estimation of the bispectrum we took a set of triangles with sides  $(k_1, k_2, k_3)$  with  $k_1 \geq k_2 \geq k_3$  going from the fundamental frequency  $k_f$  until the Nyquist wavenumber  $k_N$ . In the figure, we plot the absolute deviation with respect to the alias-free estimation versus  $k_{max} = \max(k_1, k_2, k_3)$ . We binned the data in intervals of width  $\Delta k_{max} = 0.02 \, k_N$ , we took the median, represented as a continuous line and, to represent data dispersion, we also show the first and third quartiles as a shadow region around the median. In the left panel we show the classical mass assignment schemes NGP, CIC, TSC and PCS, while for the right panel we have the modified the classical window functions, NJ1, NJ2, and NJ3.

As shown in the figure, for this new modified mass assignment scheme, we obtain an improvement in terms of the reduction of the aliasing contribution on the bispectrum with results comparable to the next-order mass assignment scheme for the progenitor function. Comparing with the results of Sefusatti et al. (2016)

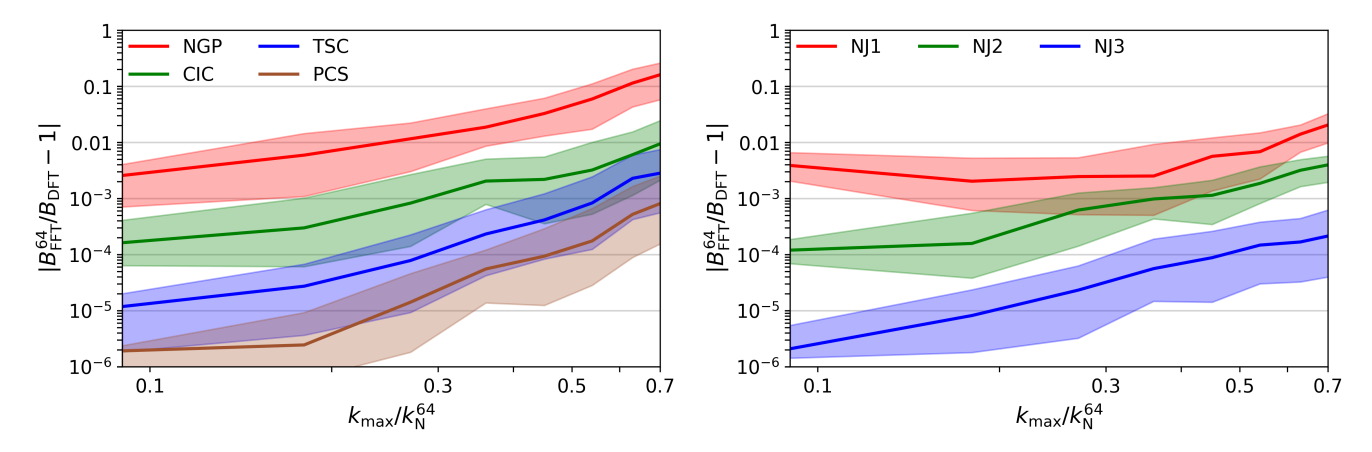
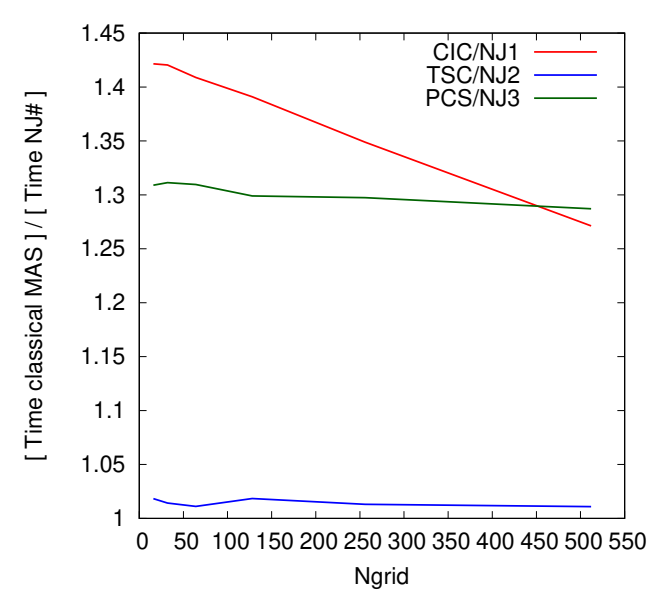


Figure 5. Aliasing contribution on bispectrum. For both panels, we display in the y-axis the absolute deviation with respect to the alias-free estimation (obtained via a direct summation). Similar to Sefusatti et al. (2016), we took a set of triangles with sides  $(k_1, k_2, k_3)$  where  $k_1 \ge k_2 \ge k_3$  going from the fundamental frequency  $k_f$  until the Nyquist wavenumber  $k_N$  and showed on the x-axis the value  $k_{max} = \max(k_1, k_2, k_3)$ . After binning the data in intervals with a width of  $\Delta k_{max} = 0.02 \, k_N$ , we took the median, represented as a continuous line and, to represent data dispersion, the first and third quartiles which are showed as a shadow around the median. In the left panel we have the classical mass assignment schemes (NGP, CIC and TSC) while in the right we have the modified classical-like window functions: NJ1, NJ2, and NJ3. All estimations were made based on the N-body simulation with parameters described in Table 1.



**Figure 6.** Ratio of the computing time of the classical MAS against the computing time of the relative (aliaswise) NJ function.

we have that our results are comparable with the bispectrum contribution at  $k_{max} \approx \frac{2}{3} k_N$ .

## 6.3. Computational performance

In order to study the computational cost of the proposed MAS with the NJ functions, we performed a set of numerical experiments.

First, in order to make a fair experiment, we used the same computing facility, and the same numerical setup was used for all simulations. Then, for a set of grid sizes of  $16^3$ ,  $32^3$ ,  $64^3$ ,  $128^3$ ,  $256^3$  and  $512^3$  we ran the estimation of the density field for each MAS (NGP, CIC, TSC, PCS, NJ1, NJ2, and NJ3) ten times for each grid size. For this experiment, we used the same simulation as described in § 5. Then, we computed the median time consumed for the code to estimate the density field for each MAS at a given grid size.

In Figure 6 we compare the mean cpu time consumed for code as a function of the grid size. Although by construction the NJ functions are related with the classical MAS as NJ1  $\rightarrow$  NGP, NJ2  $\rightarrow$  CIC, and NJ3  $\rightarrow$  TSC. As it is shown in Figure 5, the aliasing contribution of the NJ functions are comparable to the next-order interpolator, and this effect is more evident for NJ2, whose results are comparable to those of TSC (especially for large scales) and NJ3 with PCS. In Figure 6, we show the computing time ratio between CIC/NJ1, TSC/NJ2, and PCS/NJ3, since their alias contributions to the power spectrum were similar.

As it can be seen, in all cases, the ratio is close or larger than 1, which means that in each case, the performance of the NJ functions is better than the classical MAS used for comparison. For the case of PCS/NJ3 and TSC/NJ2 the ratio is almost constant, and we see an actual improvement when comparing PCS with NJ3, with PCS being  $\sim 1.3$  times slower than PCS. There is no much gain in our implementation when comparing TCS with NJ2, where it can be seen that TCS is just  $\sim 1.01$  times slower than that of NJ2. On the other hand, the ratio between the computing time of CIC against NJ1 is not constant, and changes linearly from  $\sim 1.4$  to  $\sim 1.28$ . Although in this case the ratio is not constant, this behavior appears because at increasing the grid since, the computing time per grid points is smaller (always) for NJ1, but it changes faster for CIC than for NJ1 (CIC is slower than NJ1 at lower values of the number of grid points).

This experiment confirms the benefit obtained with the use of the NJ functions, which with a comparable aliasing effect estimates the density field with a shorter computation time.

# 7. Summary and discussion

In this work we studied the impact of the mass assignment scheme on the estimation of power spectrum and bispectrum of the classical mass assignment schemes: NGP, CIC, and TSC. Based on that study, we propose a new set of MAS, the NJ functions: NJ1, NJ2 and NJ3 that are the result of classical MAS combinations.

We study the aliasing effect of for these mass assignment schemes on the power spectrum and bispectrum and we compared the results with the classical mass-assignment schemes. We obtained for the estimation of the power spectrum and bispectrum that our derived mass assignment schemes are similar or even better to the next order mass assignment scheme of the progenitor MAS, all this at expenses of a smaller computation cost and without the need of extra memory, as for example, technique described by Sefusatti et al. (2016). This gives a good perspective for the use of these new mass assignment schemes. We found also that the aliasing effect is improved even more for progenitor window functions of a higher order.

For the bispectrum we found that there is a possible trend in logarithmic scale for the aliasing contribution, which is desirable to model the bispectrum corrections. These results are very important for future studies of large scale Fourier statistics, letting to obtain great precision without the need to use extra computational resources relative to the classical mass assignment schemes.

The results presented in this work could have an interesting impact in the forthcoming years, where with the release of ongoing large scale surveys, the precise estimation of Fourier statistics of the density field in the large scales will be an important subject in the study of cosmology and LSS.

This work was supported by Universidad de Antioquia, Comité para el Desarrollo de la Investigación (CODI) project 2022-53144 and by MINCIENCIAS, research project 111571250082 (convocatoria 715-2015). The authors thank the referee for their useful comments.

## **■ REFERENCES**

Bernardeau, F., Colombi, S., Gaztañaga, E., & Scoccimarro, R. 2002, PhR, 367, 1, doi: 10.1016/S0370-1573(02)00135-7 Colombi, S., Jaffe, A., Novikov, D., & Pichon, C. 2009, MNRAS, 393, 511, doi: 10.1111/j.1365-2966.2008.14176.x Cui, W., Liu, L., Yang, X., et al. 2008, ApJ, 687, 738, doi: 10.1086/592079

Fry, J. N. 1984, ApJ, 279, 499, doi: 10.1086/161913

Gil-Marín, H., Noreña, J., Verde, L., et al. 2015, MNRAS, 451, 539, doi: 10.1093/mnras/stv961

Gil-Marín, H., Wagner, C., Fragkoudi, F., Jimenez, R., & Verde, L. 2012, JCAP, 2, 047, doi: 10.1088/1475-7516/2012/02/047

Gil-Marín, H., Wagner, C., Noreña, J., Verde, L., & Percival, W. 2014, JCAP, 12, 29, doi: 10.1088/1475-7516/2014/12/029

Hockney, R. W., & Eastwood, J. W. 1981, Computer Simulation Using Particles (New York, NY: McGraw-Hill)

Jeong, D. 2010, PhD thesis, Cosmology with high (z > 1) redshift galaxy surveys, University of Texas at Austin

Jing, Y. P. 2005, ApJ, 620, 559, doi: 10.1086/427087

Martínez, V. J., & Saar, E. 2002, Statistics of the Galaxy Distribution (Chapman & Hall/CRC)

Matarrese, S., Verde, L., & Heavens, A. F. 1997, MNRAS, 290, 651, doi: 10.1093/mnras/290.4.651

Mo, H., van den Bosch, F., & White, S. 2010, Galaxy Formation and Evolution (Cambridge, UK: CUP), doi: 10.1017/CBO97805 11807244

Peebles, P. J. E. 1980, The large-scale structure of the universe (Princeton, N.J.: Addison-Wesley)

Schmittfull, M. M., Regan, D. M., & Shellard, E. P. S. 2013, PhRVD, 88, 063512, doi: 10.1103/PhysRevD.88.063512

Scoccimarro, R. 1997, ApJ, 487, 1, doi: 10.1086/304578

--. 2000, ApJ, 544, 597, doi: 10.1086/317248

Sefusatti, E., Crocce, M., Scoccimarro, R., & Couchman, H. M. P. 2016, MNRAS, 460, 3624, doi: 10.1093/mnras/stw1229

Springel, V. 2005, MNRAS, 364, 1105, doi: 10.1111/j.1365-2966.20 05.09655.x